This is the accepted manuscript made available via CHORUS. The article has been published as:

Self-assembly of nanoparticles into heterogeneous structures with gradient material properties

Jonghyun Park and Wei Lu

Phys. Rev. E **83**, 031402 — Published 18 March 2011

DOI: 10.1103/PhysRevE.83.031402

Self-assembly of nanoparticles into heterogeneous structures with gradient material properties

Jonghyun Park and Wei Lu*

Department of Mechanical Engineering, University of Michigan, Ann Arbor, Michigan 48109, USA

Abstract

We present a mechanism to form self-assembled functional gradient superlattice structures by subjecting binary nanoparticles in an electric field. The interaction among different dipoles leads to controllable formation of diverse structures, including particle columns with gradient material properties from inside to outside and various hierarchical layered or three dimensional particle chain networks. We elucidate how permittivity, volume fraction, particle size, and the frequency of the electric field can be utilized to control the morphology of the induced structures, which would enable designed nanofabrication.

* Corresponding author. Email address: weilu@umich.edu

I. Introduction

Advanced functional materials and devices demand techniques to assemble structures at the nanometer scale [1-3]. Self-assembly is one of the most promising approaches to integrate nanoscale building blocks into desired structures. Self-assembly can be driven by various interactions such as chemical bonding [4], electromagnetic field [5], flow field [6], or capillary force [7]. The electrostatic interaction has raised significant interest because of its long-range effect and simplicity of control, which has been shown to pattern molecules [8], promote the exfoliation of nanoplates [9], and control the rotation of nanoparticles [10]. A particularly notable phenomenon is that mono-dispersed spherical particles can acquire electric moments and line up into chains parallel to an applied electric field [11]. In this process the dipolar interaction between particles plays a critical role. Studies suggest that the ground state of the chain structure is body-centered-tetragonal [12], which has been observed in simulations [13] and experiments [14]. The phase diagram of dipolar hard spheres obtained from Monte Carlo simulations shows that other phases such as disordered fluidic or close packed structures (f.c.c or h.c.p.) may also emerge [15].

Binary mixtures may provide a much richer class of nanocomposite materials. Solid mixtures of polymers at nanoscale can exhibit mechanical, optical, and electro-optical properties that are not attainable with a single polymer. Binary nanoparticle superlattices enhance the possibility of combining the properties of individual components with new functionalities that arise from the interactions between different nanoparticles. Examples include an enhancement of the energy product in nanocomposite materials by exchange coupling between nanoparticles of magnetically soft and hard materials [16]. These systems are applicable for advanced permanent

magnetic devices because they have a large energy product compared to traditional single-phase materials.

Fabrication of complex nanostructures such as core-shell, porous or monolayered structures, is challenging and requires different techniques. A heterogeneous nucleation-and-growth processing has been used to synthesis multi-component mixture of core-shell structures [17]. Another example is the synthesis of ordered mesoporous materials. Ordered mesoporous metal composite is difficult to synthesis because of high surface energies that favor low surface areas. Self-assembly of block copolymers with ligand-stabilized platinum nanoparticles has been used to generate lamellar CCM-Pt-4 and inverse hexagonal (CCM-Pt-6) hybrid mesostructures with high nanoparticle loadings [18]. Using biomolecular interaction such as DNA hybridization is another way to generate nanoscale architectures. Satellite-shaped assemblies have been constructed via DNA-directed self-assembly of gold nanoparticles [19]. Electric field has been utilized to assemble colloidal particles into two- and three-dimensional crystal structures. By adjusting the strength of an applied DC field, or strength and frequency of an AC field, it is possible to form reversible two-dimensional fluid and crystalline colloidal states on the electrode surface [20-22]. For particles distributed in a three-dimensional space, an applied electric field can cause them to aggregate into chains. These chains coarsen and eventually form thick columns [23]. Binary colloidal particles offer great potential for tuning material properties. It has been demonstrated that an AC field may produce triangular- or square superlattice particles [24], as well as large 3D single crystal with a NaCl structure [25]. An external electric field normal to the interface is capable of controlling the lattice spacing and forming defect-free monolayers [26]. There is a rich set of analogous literature in magnetic colloids due to similarity in the dipole type interactions. For instance, local crystallites with triangular and square symmetry has been

observed by ultrafast quenching of binary colloidal suspensions in an external magnetic field [27]. Thus the computational work in this paper will benefit a broader range of systems and provide guidance to the experimental investigations. Unlike monoparticles, the behavior of binary nanoparticles in an electric field is still not well understood.

We demonstrate that the various two- or three-dimensional nanostructures generated by these different techniques [17-21] can be constructed by tuning an applied electric field and controlling the particle distribution. Our simulation predicts a diverse set of nanostructures. We show that mixing two or more types of nanoparticles can open up a wide range of heterogeneous structures not possible in a mono-dispersed system. This work will explore permittivity, volume fraction, particle size, and the frequency of the applied electric field.

Diffusive motion dominates the movement of nanoparticles suspended in a quiescent liquid. We use Brownian dynamics to model the system [28]. Liquid molecules affect nanoparticles by random collisions, and imposing a frictional drag force on their motion. The trajectory of a particle at time t is governed by the Langevian equation, $m_i\ddot{\mathbf{r}}_i(t) = \mathbf{F}_i^D(t) + \mathbf{F}_i^R(t) + \mathbf{F}_i^E(t)$, where m_i and $\mathbf{r}_i$ denote the mass and position of particle i. The inertia term, $m_i\ddot{\mathbf{r}}_i$, can be neglected due to the small particle size and therefore a low Reynolds number. The forces acting on particle i include a drag force $\mathbf{F}_i^D$, a random force $\mathbf{F}_i^R$, and a force due to the electrostatic interaction $\mathbf{F}_i^E$. The Stoke's law gives $\mathbf{F}_i^D(t) = -3\pi\eta d_i \mathbf{V}_i(t)$, where η is the viscosity of the medium while d_i and $\mathbf{V}_i(t)$ are the diameter and velocity of particle i. The random force, $\mathbf{F}_i^R(t)$, represents the force causing the perpetual Brownian motion of the particles by fluctuations in the collisions with the molecules of the surrounding fluid. $\mathbf{F}_i^R(t)$ is independent of the particle velocity and varies extremely rapidly compared to the variations of the particle

velocity. The net force along the x axis, $R_{ix}(\Delta t)=\int_t^{t+\Delta t} F_{ix}^R(\xi)d\xi$, which a particle may suffer on a given occasion during an interval of time Δt, follows the distribution function $W(R_{ix}(\Delta t))=\left(2\pi q\Delta t\right)^{-3/2}\exp\left(-\left|R_{ix}(\Delta t)\right|^2/2q\Delta t\right)$ [29]. Here $q=6\pi d_i\eta k_B T$, k_B is Boltzmann's constant and T is temperature. Similar expressions exist for the random forces along the y and z axes.

Under an applied electric field $\mathbf{E}$, particle i will acquire a dipole moment of $\mathbf{p}_i=(\pi d_i^3/2)\varepsilon_m\alpha_i\mathbf{E}$. Here $\alpha_i=(\varepsilon_i-\varepsilon_m)/(\varepsilon_i+2\varepsilon_m)$, while ε_i and ε_m represent the dielectric permittivity of the particle and the medium. The dipolar interaction energy between two particles at positions $\mathbf{r}_i$ and $\mathbf{r}_j$ is given by

$$U_{ij}=\frac{1}{4\pi\varepsilon_m\left|\mathbf{r}_i-\mathbf{r}_j\right|^3}[\mathbf{p}_i\cdot\mathbf{p}_j-3(\mathbf{n}\cdot\mathbf{p}_i)(\mathbf{n}\cdot\mathbf{p}_j)], \tag{1}$$

where $\mathbf{n}$ is a unit vector in the direction of $\mathbf{r}_j-\mathbf{r}_i$. The spatial derivative of the total system energy, $(1/2)\sum_{i,j,i\neq j}U_{ij}$, gives $\mathbf{F}_i^E$.

The Reynolds number is very small for nano- and micro-particles in a liquid due to the small size, thus the inertial term can be neglected since the viscous force is so strong. This over-damping gives $m_i\ddot{\mathbf{r}}_i(t)=\mathbf{F}_i^D(t)+\mathbf{F}_i^R(t)+\mathbf{F}_i^E(t)=0$. Substituting $\mathbf{F}_i^D(t)=-3\pi\eta d_i\mathbf{V}_i(t)$ into this expression, we obtain $\mathbf{V}_i(t)=\left[\mathbf{F}_i^R(t)+\mathbf{F}_i^E(t)\right]/3\pi\eta d_i$. Applying the Euler method for time integration, where $\mathbf{V}_i(t)=\left(\mathbf{r}_i(t+\Delta t)-\mathbf{r}_i(t)\right)/\Delta t$ and Δt is time step, we obtain $\mathbf{r}_i(t+\Delta t)=\mathbf{r}_i(t)+\left[\mathbf{F}_i^R(t)+\mathbf{F}_i^E(t)\right]/3\pi\eta d_i$. This equation was implemented in our computer simulation.

II. Self-assembly of binary nanoparticle systems

Consider the electric field generated by two electrodes parallel to the $x-y$ plane at height $z=0$ and $z=h$, respectively. Between them are nanoparticles suspended in a liquid. Appling a voltage of U to the electrodes produces a uniform electric field of $E=U/h$. For those particles close to the electrodes, their dipoles cause charge redistribution in the electrode and therefore disturb the uniform field. We employ the image method to account for this effect, where image charges are placed systematically so that the isopotential condition on the electrodes can be satisfied. A dipole $\mathbf{p}_i$ at position $\mathbf{r}_i=(x_i,y_i,z_i)$ produces an infinite number of image dipoles at positions $(x_i,y_i,-z_i)$ and $(x_i,y_i,2kh\pm z_i)$ as shown in Fig. 1, where $k=\pm1,\pm2,\ldots$ is a non-zero integer. These image dipoles interact with all particle dipoles in-between the electrodes based on Eq. (1). We assume that the particles and the electrodes are "hard", and introduce a short-range repulsive force between them to ensure no material penetration. We adopt a combination of Verlet list and cell list method [30] with a cut-off length for interaction calculation. This cutoff length also determines the necessary range of k for the image dipoles.

We use A and B to denote the two types of particles. Define a length scale by the particle diameter d_A. The competition between the electrostatic and the drag force defines a time scale, $\tau=\eta/(\varepsilon_m(\alpha_A E)^2)$, where $\alpha_A=(\varepsilon_A-\varepsilon_m)/(\varepsilon_A+2\varepsilon_m)$ and $\alpha_A E$ can be treated as an effective electric field. The electrostatic force versus the random force defines a dimensionless number, $\Lambda=d_A^{3/2}\varepsilon_m(\alpha_A E)^2/\sqrt{\eta k_B T/\tau}$ or $\Lambda=d_A^{3/2}|\alpha_A|E\sqrt{\varepsilon_m/k_B T}$. A larger electric field or particle diameter reduces the relative effect of Brownian motion. Brownian motion can shake the particles to avoid them being trapped at a local minimum configuration. On the other hand, a system may lose its order when Λ is too small, i.e. significant Brownian motion. Thus an

appropriate Λ helps to form a more ordered structure. We perform simulations using the normalized length and time with periodic boundary conditions in the *x* and *y* directions.

Define the permittivity ratios of A and B particles to that of the medium by $\beta_A = \varepsilon_A / \varepsilon_m$ and $\beta_B = \varepsilon_B / \varepsilon_m$. The direction of an induced dipole is along ($\beta > 1$) or opposite ($\beta < 1$) to the applied field. According to Eq. (1), the interactive energy between two particles with dipoles p_1 and p_2 is proportional to $p_1 p_2 (1 - 3\cos^2\theta)$, with θ being the angle between the direction along the centers of two particles and the applied field. For a monodispersed system composted of A particles only, the product $p_1 p_2 = p_A^2$ is always positive no matter whether the particle is more polarizable than the medium or not. Thus the energy will always be minimized when two particles line up along the direction of the electric field so that $\theta = 0$ or π. As a result, particles form chains bridging the electrodes.

For a binary system, however, the chain formation is strongly dependent on the polarization capability of the particles relative to that of the surrounding medium. There are two cases: case I, both particles are more ($\beta_A, \beta_B > 1$) or less ($\beta_A, \beta_B < 1$) polarizable than the medium; or case II, one type of particle is more polarizable than the medium ($\beta_A > 1$) while the other is less polarizable ($\beta_B < 1$).

In case I the interactive energy between two particles, which is proportional to $p_1 p_2 (1 - 3\cos^2\theta)$, minimizes when $\theta = 0$ or π since $p_1 p_2 > 0$. Thus particles tend to form a chain along the direction of the field. A single chain will form when the length of all particles lined-up together is less than *h*. Given sufficient number of particles, multiple chains emerge. Will a chain prefer to be composed of a single type of particles or be a mixture of two types of particles? To address this question, consider a chain of repetitive units that are composed of A

and B particles, as shown in Fig. 2. Each unit contains N particles. The number of A and B particles is assumed equal. We calculate the interactive energy among the N particles in one unit, U_1, and the interactive energy between these N particles and those particles outside this unit, U_2. The energy per unit is given by $U(p_A, p_{B,} N) = U_1 + U_2 / 2$, which depends on the dipole moments of the two types of particles, p_A, p_B, and the length of the unit N. The coefficient 1/2 appears in the second term since a unit shares one half of its interactive energy with another unit. The average energy per particle is $u(p_A, p_{B,} N) = U / N$. The configuration with lower u is energetically favorable. Denote the average energy corresponding the smallest unit length (N=2) by u_0. The $(u - u_0) / |u_0|$ curves in Fig. 2 show that the free energy of the system decreases with N. Thus same types of particles tend to get together, or the system does not like mixing particles in a chain. This effect becomes stronger when the difference between the dipole moments of A and B is larger. When there are a small number of particles so that only one chain can form, the configuration with the lowest energy is a chain of two segments. One segment is composed of A while the other is composed of B. Multiple chains will form when there are many particles to bridge the gap between the two electrodes. In this case the system prefers to form pure chains, each composted of only one type of particles. Based on the particle type, we refer them as A chain and B chain.

In case II, however, the opposite polarization direction of A and B particles leads to an interactive energy scaling as $-|p_A p_B|(1 - 3\cos^2\theta)$. Thus the energy is minimized at $\theta = \pi / 2$, or A and B particles prefer to stay in a plane perpendicular to the applied field and attract each other. Same types of particles will line up along the electric field to form A or B chains. While the system prefer to form pure particle chains in both case I and II, the geometric relations between

chains are different. Fig. 3 illustrates the relative position of two chains. In Fig. 3a, A and B particles have the same polarization direction. Thus they will repel each other if they stay in a plane perpendicular to the electric field. The interaction becomes attractive if two particles shift relative to each other by $d/2$. This configuration has lower energy. In Fig. 3b, A and B particles have opposite polarization directions and the shown parallel configuration has lower energy.

III. Simulation results

Representative results are shown in Fig. 4. Both three-dimensional views (left) and the middle cross-section views (right) are given. The systems were allowed to evolve for a sufficiently long time until no significant changes in the potential energy could be observed. The two types of particles A and B are represented by the red (light gray) and blue (dark gray) colors, respectively. They have the same diameter d. The distance between the top and bottom electrodes is $14d$. The calculation domain size is $27d \times 27d \times 14d$ with periodic boundary conditions in the x and y directions. The number of A and B particles are equal. Fig. 4a and 4b demonstrate a case that both particles are more polarizable than the medium, where $\beta_A = 50$ and $\beta_B = 5$. The system in Fig. 4a has a total of 2000 particles, which corresponds to a volume fraction of 10.3 %. The particles assemble into isolated columns with a core-shell configuration. The core is composed of the more polarizable A particles, while the shell is composed of B. From an energetic point of view, the attraction between two A chains is stronger than that between the A and B chain. As a result, the A chains aggregate to form A columns. The B chains tend to get as close to the A columns as possible, leading to the formation of B shells. It is important to note that this self-organized functionally gradient structure offers a gradual transition of the permittivity from the core to that of the medium. This approach could be

potentially very useful to construct functional gradient nanocomposites from bottom up. Fig. 4b shows the results for a higher volume fraction of particles. There are a total of 6000 particles, giving a volume fraction of 30.8 %. The system evolves into a continuous structure with isolated holes in between. The B particles enclose the A particles, and form the peripheral regions around the holes.

Fig. 4c demonstrates a case where one type of particle is more polarizable than the medium while the other is less polarizable. All parameters are the same as those in Fig. 4a except that now $\beta_A = 2.8$ and $\beta_B = 0.28$. The particles also form pure chains along the field direction. A distinct feature in Fig. 4c is that A and B chains are highly dispersed and form a network of alternating A and B particles in the *x*-*y* plane. This morphology is in contrast to that in Fig. 4a, where the same type of chains aggregate. As mentioned before, the opposite dipole directions cause A and B particles to attract each other in the *x*-*y* plane. While same type of particles repel each other, leading to a dispersed alternating chain distribution. Simulations of different combinations of β_A and β_B lead to the phase diagram in Fig. 5, which shows the cross-section view of different nanostructures. These bulk structures are three dimensional and extend along the electric field direction.

A challenge to generate well-organized superlattices of binary particles is to avoid being trapped at the local energy minimum. We have found that an annealing process can facilitate the formation of ordered structures. Fig. 6a shows the mean square displacement, $\langle r^2 \rangle$, which contains information on the particle diffusivity. Here < . > denotes averaging over all particles. When the system solidifies, the mean square displacement saturates to a certain value and $\langle r^2 \rangle / t$ approaches zero. If the system is liquid, the mean square displacement grows linearly with time so that $\langle r^2 \rangle / t$ approaches a finite value. From the figure we find that the A particles become

solidified and well-ordered due to their larger permittivity. However, the B particles which have less permittivity are still in a liquid state due to their weak interactions. The annealing process is achieved by decreasing the temperature (or increasing the electric field) to a certain level and hold it for some time. The A particles form crystal structures first. Then, through annealing, the B particles also form similarly well-organized superlattices. Fig. 6b shows the structure formed by an annealing process. As can be seen, the structures in Fig. 6b are more regular than those in Fig. 4a. Note that in the simulation the hydrodynamic effect when a particle moves in the liquid is considered in terms of the Stokes' drag force of an isolated particle. We have neglected the hydrodynamic interaction between two particles. This assumption greatly simplifies and facilitates the simulation by avoiding complex fluid dynamics calculations, and therefore allows simulating many particles in a practical amount of time. However, this assumption is only valid when the flow fields around the two particles do not interference each other too much. The interaction becomes important when the separation between two particles is comparable to the size of the particle. The close particles would result in cooperative diffusion [31] and significantly modify the kinetics of the structuring process.

Assembling a single layer of nanoparticles on a substrate has many potential applications. Figure 7 shows the self-assembly of a layer of two types of particles on a surface. The parameters are the same as those in Fig. 4a except that the diameter of the red (light gray) A particles is three times of that of the blue (dark gray) B particles. The system has 16 A particles among a total of 200. The induced dipole moment increases quickly with the particle diameter. Thus stronger interactions between A particles are expected. The A and B particles are placed randomly. Fig. 7a shows the structure formed under an out-plane electric field perpendicular to the surface. The repulsion between the A particles causes them to organize into a nicely ordered

triangular lattice. The attraction between the A and B particles causes the formation of B rings surrounding the A cores. Figure 7b shows the structure under an in-plane electric field. The red (light gray) A particles form a chain along the field direction first. Then the blue (light gray) B particles form side chains and attach to the A particle chains.

In general, nanoparticles and the surrounding medium are not ideal dielectrics. The response of a lossy dielectric to an external field depends on the frequency since the material's polarization does not respond instantaneously to the applied field. For an alternating electric field we must take into account the finite electric conductivity. The dependence on field frequency provides a powerful approach to control the morphologies. The complex effective dipole moment is given by $\mathbf{p}_i = (\pi d_i^3/2)\varepsilon_m \tilde{\alpha}_i \mathbf{E}$, where $\tilde{\alpha}_i = (\tilde{\varepsilon}_i - \tilde{\varepsilon}_m)/(\tilde{\varepsilon}_i + 2\tilde{\varepsilon}_m)$ and $\tilde{\varepsilon}_i = \varepsilon_i + \sigma_i / j\omega$, $\tilde{\varepsilon}_m = \varepsilon_m + \sigma_m / j\omega$. Here ω is the angular frequency of the electric field, $j = \sqrt{-1}$, σ_i and σ_m are the conductivity of particle i and the medium. The angular frequency relates to the ordinary frequency f (Hz) by $\omega = 2\pi f$. The interactive energy between particle i and j is $U_{ij} = -\mathrm{Re}[\mathbf{p}_i^* \cdot \mathbf{E}_j]$. Here $\mathbf{p}_i^*$ denotes the complex conjugate of $\mathbf{p}_i$. The induced field at position $\mathbf{r}_i$ by dipole $\mathbf{p}_j$ is $\mathbf{E}_j = \left(3\mathbf{n}(\mathbf{p}_j \cdot \mathbf{n}) - \mathbf{p}_j\right) / \left(4\pi\varepsilon_m \left|\mathbf{r}_i - \mathbf{r}_j\right|^3\right)$ [32]. Consequently, we have an expression similar to Eq. (1). Using $\cos\theta = \mathbf{n} \cdot \mathbf{E}$, the time averaged interaction between two lossy particles is

$$U_{ij} = \frac{\pi d_i^3 d_j^3 \left(1 - 3\cos^2\theta\right)\varepsilon_m E_{rms}^2}{16\left|\mathbf{r}_i - \mathbf{r}_j\right|^3} \mathrm{Re}[\tilde{\alpha}_i^* \tilde{\alpha}_j], \tag{2}$$

where E_{rms} indicates the root mean square of $|\mathbf{E}|$. Note that the factor, $\mathrm{Re}[\tilde{\alpha}_i^* \tilde{\alpha}_j]$, can be positive, negative, or zero depending on the frequency.

In Fig. 8a, Re[$\tilde{\alpha}_i^* \tilde{\alpha}_j$] is plotted for the strontinum-titanate nanoparticle (A) and the zeolite nanoparticle (B) in silicone oil. The strontinum-titanate particle has a dielectric constant of $\varepsilon_{rA} = 294$ and a conductivity of $\sigma_A = 2\times10^{-8}$ S/m [33]. The relation between dielectric permittivity and dielectric constant is $\varepsilon_A = \varepsilon_{rA}\varepsilon_0$, where ε_0 = 8.85×10^{-12} F/m is vacuum permittivity. The humidified zeolite particles used in our simulations have a dielectric constant of ε_{rB}=23.7 and a conductivity of $\sigma_B = 1.5\times10^{-5}$ S/m [34]. The dielectric constant and conductivity for silicone oil are ε_{rm}=2.54, and $\sigma_m = 10^{-13}$ S/m [33], respectively. In our simulations these values were used to calculate $\tilde{\varepsilon}_A = \varepsilon_A + \sigma_A / j\omega$, and similarly $\tilde{\varepsilon}_B, \tilde{\varepsilon}_m$. These complex permittivity then gave $\tilde{\alpha}_A = (\tilde{\varepsilon}_A - \tilde{\varepsilon}_m)/(\tilde{\varepsilon}_A + 2\tilde{\varepsilon}_m)$ and similarly $\tilde{\alpha}_B$. The three Re[$\tilde{\alpha}_i^* \tilde{\alpha}_j$] curves show the interactive energy between A and A (Re[$\tilde{\alpha}_A^* \tilde{\alpha}_A$]), B and B (Re[$\tilde{\alpha}_B^* \tilde{\alpha}_B$]), A and B (Re[$\tilde{\alpha}_A^* \tilde{\alpha}_B$]). Note that Re[$\tilde{\alpha}_A^* \tilde{\alpha}_B$]=Re[$\tilde{\alpha}_B^* \tilde{\alpha}_A$].

In the low frequency region I, Re[$\tilde{\alpha}_i^* \tilde{\alpha}_j$] is positive so that the interactive energy between A and B is minimized at $\theta = 0$ or π. This situation is similar to Fig. 4a. In a specific frequency range, as shown by the shaded region II in Fig. 8a, the interaction between A and B is very weak. At these frequencies the two types of particles will form chains independently. In other words, there is not much interaction between A and B chains. However, the interaction between same type of chains, e.g. A toA, or B toB, is still strong. At high frequency region III, Re[$\tilde{\alpha}_i^* \tilde{\alpha}_j$] becomes negative. The interactive energy between A and B is minimized at $\theta = \pi / 2$, which is similar to the situation in Fig. 4c. Thus tuning the frequency can change the interaction between two types of particles and therefore the formed structures. Figure 8b shows an example demonstrating the result after shifting the frequency from region II to III. Initially A and B

particles align and form chains independently. Same type of chains will get together to form A columns or B columns, since the interaction among same types of particles is still strong. After the electric field frequency is shifted higher, A and B columns start to attract each other. The produced structure is different from that in Fig. 4c. The large columns are alternating in Fig. 8b, while single chains are alternating in Fig. 4c.

IV. Conclusions

In summary, this paper has demonstrated structures formed by binary nanoparticles in an electric field. We have shown that dipole interactions among different type of particles can lead to diverse configurations with gradient properties. The simulations have revealed rich dynamics during the structure formation process and suggested a significant degree of experimental control. The presented work can be extended to multiple particle types. Effective approaches to organize different nanoparticles systematically into ordered superlattices may enable a wide range of applications from advanced functional materials with gradient dielectric and optical properties to sensors or energy storage and conversion devices. The predicted structures may provide some critical insight into designing materials for making such engineered structures feasible.

Acknowledgements

The authors acknowledge financial support from National Science Foundation Award No. CMMI-0700048.

References

[1] A. P. Alivisatos, Science **271**, 933 (1996).

[2] S. A. Maier, Nat. Mater. **2**, 229 (2003).

[3] J. Hoinville, J. Appl. Phys. **93**, 7187 (2003).

[4] X. J. Huang, Y. Li, H. S. Im, O. Y, J. H. Kim, D. Y. J, S. O. Cho, W. P. Cai, and Y. K. Choi, Nanotechnology **17**, 2988 (2006).

[5] M. Tanase, D. M. Silevitch, A. Hultgren, L. A. Bauer, P. C. Searson, G. J. Meyer, and D. H. Reich, J. Appl. Phys. **91**, 8549 (2002).

[6] W. Salalha, and E. Zussman, Phys. Fluids **17**, 063301 (2005).

[7] R. A. Richard, A. Syms, V. M. Bright, and G. M. Whitesides, J. Microelectromechanical systems **12**, 387 (2003).

[8] W. Lu, and D. Salac, Phys. Rev. Lett. **94**, 146103 (2005).

[9] W. Lu, H. Koerner, and R. Vaia, Appl. Phys. Lett. **89**, 223118 (2006).

[10] J. Park, and W. Lu, Appl. Phys. Lett. **91**, 053113 (2007).

[11] M. Parthasarathy, and D. J. Klingenberg, Mat. Sci. Eng. **R17**, 57 (1996).

[12] R. Tao, and J. M. Sun, Phys. Rev. Lett. **67**, 398 (1991).

[13] R. Tao, and Q. Jiang, Phys. Rev. Lett. **73**, 205 (1994).

[14] T. Chen, R. N. Zitter, and R. Tao, Phys. Rev. Lett. **68**, 2555 (1992).

[15] A.-P. Hynninen, and M. Dijkstra, Phys. Rev. E **72**, 051402 (2005).

[16] H. Zeng, J. Li, J. P. Liu, Z. L. Wang, and S. Sun, Nature **420**, 395 (2002).

[17] Y. F. Tang, Z. P. Huang, L. Feng, and Y. F. Chen, Appl Surf Sci, 412 (2005).

[18] S. C. Warren, L. C. Messina, L. S. Slaughter, M. Kamperman, Q. Zhou, S. M. Gruner, F. J. DiSalvo, and U. Wiesner, Science **320**, 1748 (2008).

[19] H. Yao, C. Yi, C.-H. Tzang, J. Zhu, and M. Yang, Nanotechnology **18**, 015102 (2007).

[20] M. Trau, D. A. Saville, and I. A. Aksay, Science **272**, 706 (1996).

[21] M. Bohmer, Langmuir **12**, 5747 (1996).

[22] T. Gong, and D. W. M. Marr, Langmuir **17**, 2301 (2001).

[23] W. Wen, D. W. Zheng, and K. N. Tu, J. Appl. Phys. **85**, 530 (1999).

[24] W. D. Ristenpart, I. A. Aksay, and D. A. Saville, Phys. Rev. Lett. **90**, 128303 (2003).

[25] E. C. M. Vermolen, A. Kuijk, L. C. Filion, M. Hermes, J. H. J. Thijssen, M. Dijkstra, and A. v. Blaaderen, PNAS **106**, 16063 (2009).

[26] N. Aubry, P. Singh, M. Janjua, and S. Nudurupati, PNAS **105**, 3711 (2008).

[27] L. Assoud, F. Ebert, P. Keim, R. Messina, G. Maret, and H. Lowen, Phys. Rev. Lett. **102**, 238301 (2009).

[28] M. P. Allen, and D. J. Tildesley, *Computer simulation of liquids* (Clarendon Press, Oxford, 1987).

[29] S. Chandrasekhar, Rev. Mod. Phys. **15**, 1 (1943).

[30] D. Frenkel, and B. Smit, *Understanding Molecular Simulation* (Academic Press, San Diego, 2002).

[31] G. Nagele, J. Bergenholtz, and J. K. G. Dhont, J Chem Phys **110**, 7037 (1999).

[32] J. D. Jackson, *Classical Electrodynamics* (John Wiley & Sons, Inc., New York, 1999).

[33] Z. Y. Wang, R. Shen, X. J. Niu, G. Sun, K. Q. Lu, B. Hou, and W. J. Wen, J Phys D Appl Phys **38**, 1325 (2005).

[34] C. W. Wu, Y. Chen, and H. Conrad, J Phys D Appl Phys **31**, 960 (1998).

Figure Captions

Fig. 1 A configuration of particles between two electrodes (top), and the corresponding dipoles and image dipoles (bottom). The infinite pattern shows a periodicity of $2h$.

Fig. 2 Shown is the change of the average energy per particle as a function of unit length. The free energy of the system decreases with N. Thus same types of particles tend to get together, or the system does not like mixing particles in a chain. This effect becomes stronger when the difference between the dipole moments of A and B is larger.

Fig. 3. The configuration relation between two chains. (a) A and B have the same polarization direction. They repel each other in a plane perpendicular to the electric field. The interaction becomes attractive if the two particles shift relative to each other by d/2. This configuration has lower energy. (b) A and B have opposite polarization directions. The parallel configuration has lower energy.

Fig. 4. (Color online) Three-dimensional (left) and middle cross-section views (right) of structures formed by A, red (light gray) particles and B, blue (dark gray) particles. In (a), (b) both particles are more polarizable than the medium. $\beta_A = 50$, $\beta_B = 5$, $\Lambda = 175$. (a) A volume fraction of 10.3% (2000 particles) leads to isolated columns with a core-shell configuration and thus gradient properties from inside to outside. (b). The system forms a continuous structure with isolated holes in between when the volume fraction is 30.8% (6000 particles). (c) A is more polarizable than the medium while B is less. $\beta_A = 2.8$, $\beta_B = 0.28$. Other parameters are the same as (a). The system forms highly alternating A and B chains.

Fig. 5. (Color online) A phase diagram in the parameter space of β_A and β_B shows the cross-section view of formed nanostructures.

Fig.6. (a) (Color online) The evolution of mean square displacement/time, $\langle r^2 \rangle / t$, at parameters $\beta_A = 50$, $\beta_B = 5$, $\Lambda = 100$, and volume fraction of 10.3 %. (b) Structures formed after annealing. $\Lambda = 500$.

Fig. 7. (Color online) Self-assembly of a layer of binary particles on a surface (a) under an out-plane electric field perpendicular to the surface, and (b) under an in-plane electric field. $\beta_A = 50$, $\beta_B = 5$, $\Lambda = 50$. A total of 200 particles.

Fig. 8. (a) (Color online) The effect of electric field frequency calculated for strontinum-titanate nanoparticle (A) and zeolite nanoparticle (B). $\omega = 2\pi f$ where f (Hz) is the ordinary frequency. (b) Structure formed after initial self-assembly in region II followed by further evolution in region III. $\Lambda = 50$, volume fraction of 10.3 % (2000 particles).

Figures

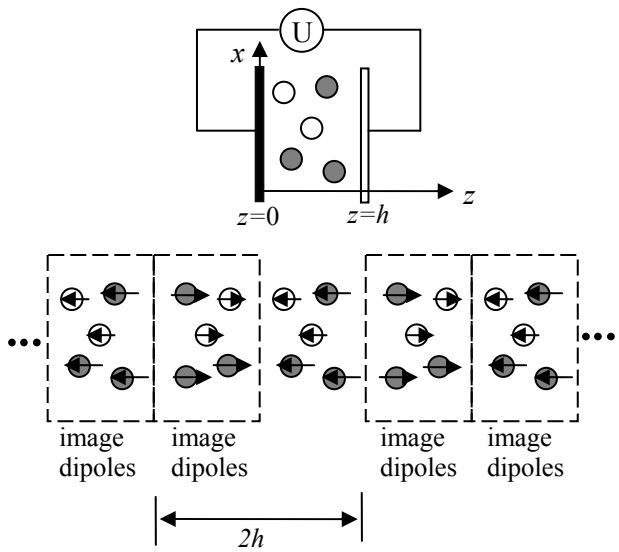

Figure 1

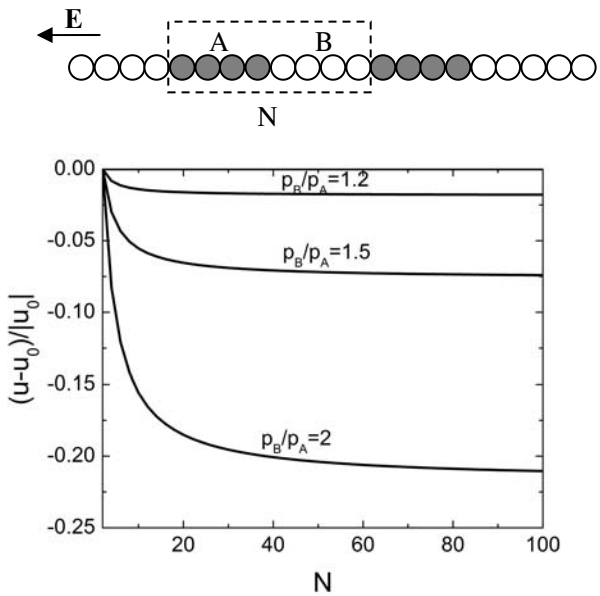
E
A
B
N
0.00
-0.05
-0.10
-0.15
-0.20
-0.25
$(u-u_0)/|u_0|$
p_B/p_A=1.2
p_B/p_A=1.5
p_B/p_A=2
20
40
60
80
100
N

Figure 2

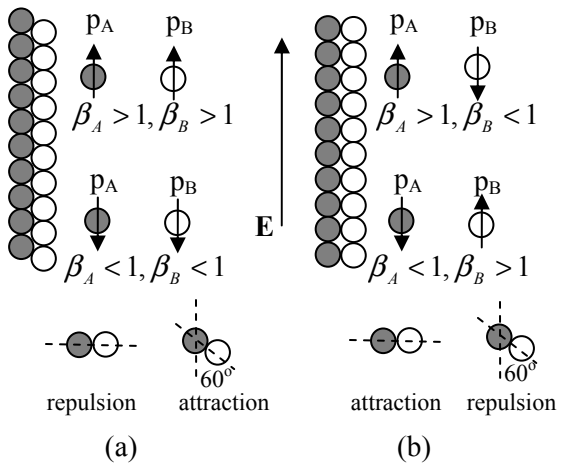
pA
pB
$\beta_A > 1, \beta_B > 1$
pA
pB
$\beta_A < 1, \beta_B < 1$
E
pA
pB
$\beta_A > 1, \beta_B < 1$
pA
pB
$\beta_A < 1, \beta_B > 1$
60°
repulsion
attraction
60°
attraction
repulsion
(a)
(b)

Figure 3

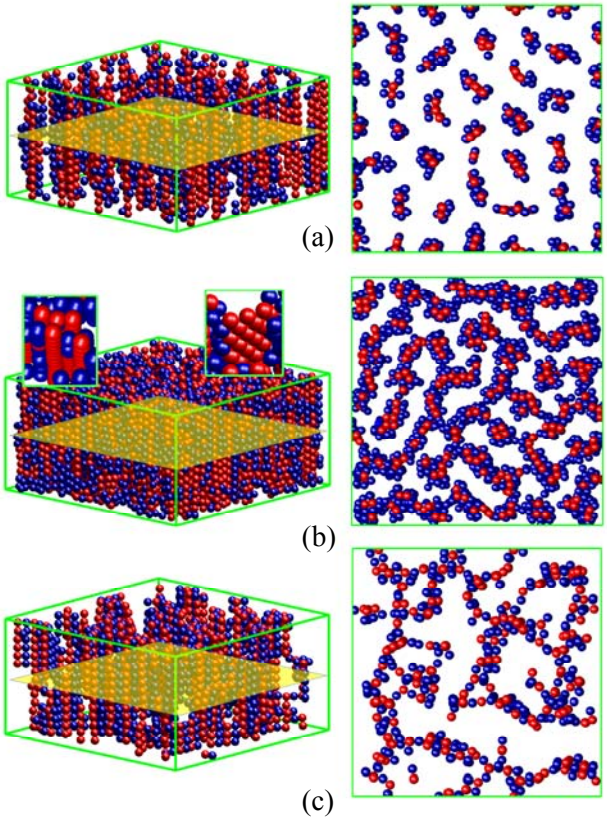

Figure 4

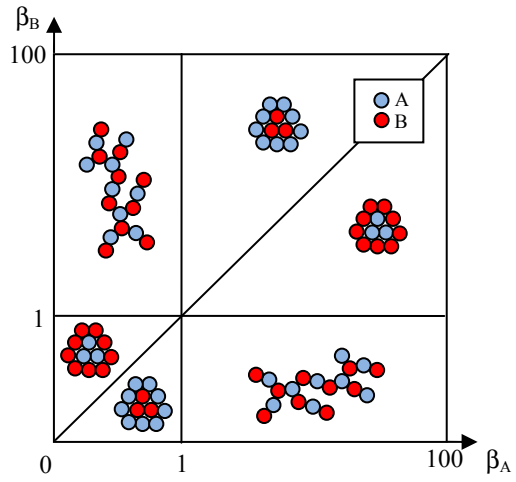

Figure 5

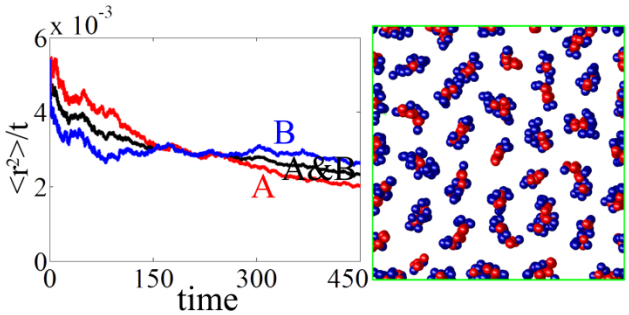

(a) (b)

Figure 6

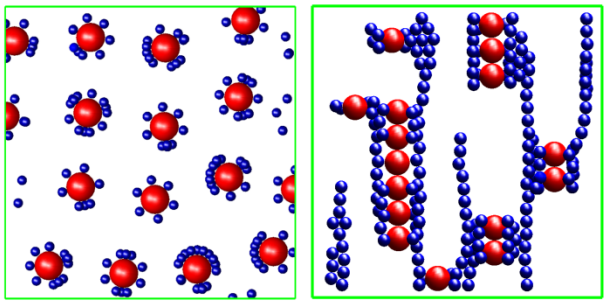

(a) (b)

Figure 7

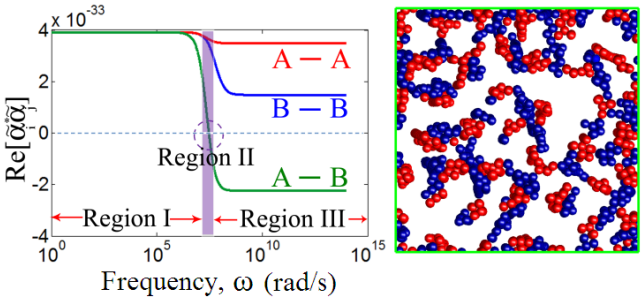
x 10^-33
4
2
0
-2
-4
Re[α̃α̃*]
A — A
B — B
A — B
Region II
Region I
Region III
10^0
10^5
10^10
10^15
Frequency, ω (rad/s)

(a) (b)

Figure 8